Iran University of Science and Technology

International Journal of

Railway Research

ISSN: 2423-3838

Nonlinear Train-Track-Bridge Interaction with Unsupported Sleeper Group

Reza Naseri[1], Saeed Mohammadzadeh[1*]

[1]School of Railway Engineering, Iran University of Science and Technology, Tehran, Iran

ARTICLE INFO

Article history:
Received: 23.02.2020
Accepted: 1.04.2020
Published: 26.06.2020

Keywords:
Train-tack-bridge system
Railway bridge dynamic
Unsupported sleeper
Wheel/rail interaction
Finite element method

A B S T R A C T

One of the main characteristics of the ballasted track compared to the slab track is the ability to reduce the level of vibration on the bridge surface. However, due to factors such as the asymmetric or permanent settlement of the ballast layer (compaction), crushing, or moving of ballast particles, a gap between sleeper and ballast appears. This problem intensifies vibrations in the track and, as a result, can affect the dynamic response of the bridge. So far, the lack of scientific attention to this issue on the railway bridge is noticeable. Hence, in this article, by examining a nonlinear dynamic model of Train-Track-Bridge interaction, the effect of the unsupported sleeper on the dynamic behavior of a concrete railway bridge is studied. For this purpose, the influence of a suspended sleeper-group at the different positions along the bridge span, in a range of train speed and gap size, are investigated. It is demonstrated that for the case of the unsupported sleeper-group within the 2/8 and 5/8 of the bridge span, the acceleration of the bridge reaches its maximum. Also, the maximum load on the deck of the bridge increases by 45 to 60%.

1. Introduction

In the ballasted railway track, the vibration of the track due to the passing of various traffic loads distributes ballast particles. Under the repetition of this process, the level of ballast, along with the track changes. Moreover, due to the moving of ballast particles from one section to another, compaction of the ballast beneath some sleeper is unavoidable. During the track operation, this process will be repeated under different conditions of train speed, axle loads, weather conditions, and as a result, a gap between some sleepers and the ballast beneath them will appear. Therefore, some sleepers will no longer be fully supported by the ballast, and the ideal connection between these two elements will be omitted. This phenomenon is called the unsupported sleeper. Augustin et al [1] and Li and Sun [2] found that up to 50 % of all sleepers that they had investigated on several railway tracks are more or less unsupported. From a review of existing literature, it becomes clear that the effect of the unsupported sleeper on railway components is studied, while most of them attributed to track dynamic response. Augustin et al [1] indicated that the speed of the train and the initial imperfection, as two key factors, play a significant role in the separation between sleeper and ballast. During the operation of the track, the size of the gap increases and affects the side sleepers. It causes the number of suspended sleepers to increase. Lammering and Plenge [3] considered the suspended sleepers as a long-term cause of fatigue in the track. In general, studies on the effect of unsupported sleepers on different parts of the rail transportation system can be divided into several categories (Figure 1):

1.1 Effect of the unsupported sleeper on the train's dynamic reaction

*Corresponding author, Associate professor
Email: mohammadz@iust.ac.ir

The comfort index and safety issues, such as the train derailment, are vital factors in the survival of the railroad's popularity in comparison to other modes of transportation. Accordingly, the design engineers have always studied the effect of various conditions that track structure experiences during its operation on different parts of the train. Zhu et al [4] studied the effect of unevenly supported sleepers at two ends on the rolling response of the train bogie by using the central finite difference method. Their results displayed that suspended sleepers can have a significant impact on wheel rolling equations, which could result in the lateral instability of the wheel-sets, which increases the possibility of derailment.

1.2 Effect of the unsupported sleeper on the track component dynamic reaction

Studies on the impact of suspended sleepers on track responses have been reasonably extensive. Zhang et al [5] investigated the effect of the number of unsupported sleepers on the wheel/rail contact and discovered a dramatic increase in the maximum contact force. They found that the amount of interaction force under the 5 to 6 suspended sleepers resulted in the highest value. Zhu et al [6], through experiments, found that in the case of three unsupported sleepers, as the train speed increases from 160 to 320Km/h, the acceleration of the sleeper and ballast increases by a factor of 3.5 to 4. Following these results, with the increase of unsupported sleepers from 0 to 3, at the train speed of 320Km/h, the acceleration of sleeper and ballast increases by approximately 8 and 6.8 times, respectively. Lundqvist and Dahlberg [7] examined the effect of a 1 mm gap between sleeper and ballast. According to the results obtained in the vicinity of suspended sleepers, the interaction force between supported sleepers and ballast increased by 70 %, and displacement of the sleeper adjacent to the unsupported sleeper increased by 40 %. Bezin et al [8] investigated a finite element model of unsupported sleepers using a three-dimensional model of wheel-rail contact. According to the results, one unsupported sleeper can lead to increases of 10 to 30 % in wheel-rail contact force and 30 to 60 % in rail-sleeper contact force. Sadeghi et al [9] found that with an increase of 0.4 mm in the gap size of the hanging sleeper, the interaction force between sleeper and ballast increased by 25%.

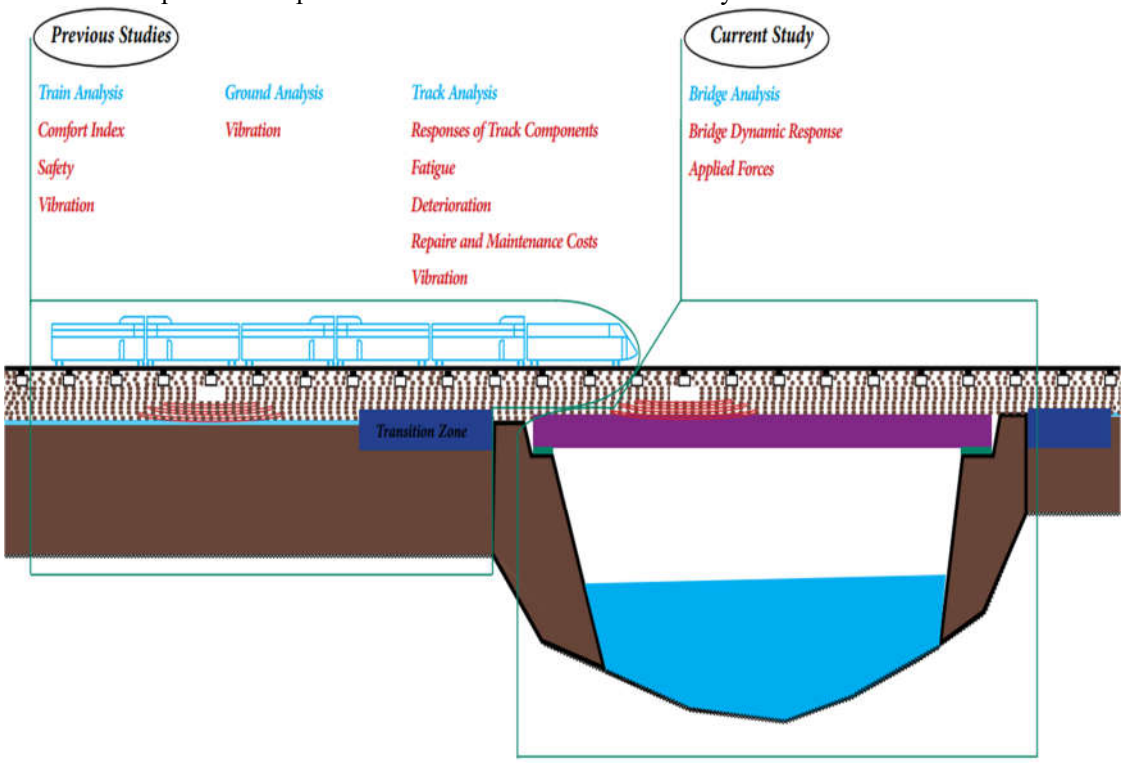

Figure 1. A comparison between the previous studies and the current research

Ishida et al [10] studied the effect of the unsupported sleeper on the bending fatigue of rail weld. According to this study, in the case of two unsupported sleepers with a 2 mm gap in the track structure, the estimated fatigue life of rail weld can fall to half of its normal life. Zakeri et al [11] compared the effect of unsupported and partially supported sleepers on the dynamic response of the track using the Finite Element Method (FEM). They discovered that as sleeper spacing increased from 50 to 75 cm, for unsupported and partially supported sleepers, the displacement of rail increased from 7 to 22 % and 5 to 8 %, respectively. Also, by changing the number of both sleepers from 1 to 9, the displacement of rail increased from 13 to 74 % and 6 to 24 % for the two cases, respectively. Dai et al [12] determined that as the space between two unsupported sleeper groups increases, the magnitude of wheel/rail contact force decreases rapidly to a case similar to the contact forces associated with an unsupported sleeper group. Also, it was found that the maximum of wheel-rail contact force generally happens on the sleeper before the first unsupported sleeper and just after the suspended sleeper group. Zakeri et al [13] by studying the effect of pad stiffness and axle loads on the dynamic response of track, considering the unsupported sleeper with a 0.8mm gap, concluded that with increasing the axle load from 12.5 KN to 25 KN, the displacement increases by 13 % and there is an inverse relationship between the pad stiffness and the rail displacement.

1.3 Effect of the unsupported sleeper on the foundation reaction

Due to the impact forces between unsupported sleepers and ballast, and also increasing the sleeper-ballast contact force in the vicinities of suspended sleepers when the wheel is passing on the hanging section, a wide range of vibrational waves are produced in the track layers. Vibrational waves are reached by the upper layer to the lower layers and affect different depth of the track and foundation structures. Esmaeili et al [14] investigated the effects of hanging sleepers on ground vibration using the train-track dynamic interaction model and the finite element model of ground-borne vibration. In this study, by examining the response of environmental vibration velocity under the different conditions of track support stiffness, a relationship was presented to calculate the maximum environmental vibration velocity. Considering the unsupported sleepers at the bridge transition zone, Stark et al [15], using the finite element software LS-DYNA concluded that the wheel force redistributed between the adjacent sleepers of the unsupported sleepers, and for the case of a 1 mm gap, the force applied to the well-supported sleeper can be increased by up to 83%. Also, at the transition zone of bridges, the wheel force can be increased by up to 25%.

1.4 In this study

A review of literature on unsupported sleepers reveals that by increasing the track forces, the rate of track deterioration will be enhanced. It can affect the dynamic performance of railway bridges. It is also found that the vibration response of concrete bridges due to the unsupported sleepers has not been attempted. Therefore the present study proposes a new approach to this subject that is schematically presented in Figure 1.

2.Modeling of Train-Track-Bridge Interaction (TTBI) and the Solution Algorithm

To study the dynamic responses of railway bridges, a coupled model consisting of two lower and upper subsystems is considered. The two subsystems are linked by using the interaction force between the wheels and the rail. Also, to complete the model, a sample of vertical roughness taken by the track recording car, EM120, is used as random irregularities within the model. The unsupported sleeper model is entered into the analysis, and the system dynamic equations are solved in an iteration algorithm by using the Newmark-β numerical solution method.

2.1 The upper subsystem model

The upper subsystem consists of several moving vehicles. The most important feature of this subsystem is that its position varies over time compared to the lower subsystem. In this study, to model the upper subsystem, the dynamic equation of rigid bodies is used. Each vehicle consists of a car-body and two bogies with two degrees of vertical and rotational freedom for each component and four wheel-sets with a degree of vertical freedom. The car body, the bogies, and the wheels are linked to each other with linear spring-damper elements, as

shown in Figure 2. With the assumption that the responses of each vehicle are considered independently of each other, the dynamic equations of each part of the vehicle can be expressed as in the following forms.

For the vertical and pitch motions of the car body:

$$\begin{aligned} &M_c\ddot{v}_c+\left[\left(\dot{v}_c-\dot{v}_{t1}\right)+\left(\dot{v}_c-\dot{v}_{t2}\right)\right]C_{s2} \\ &+\left[\left(v_c-v_{t1}\right)+\left(v_c-v_{t2}\right)\right]K_{s2}=-M_cg \end{aligned} \quad (1)$$

$$\begin{aligned} &J_c\ddot{\theta}_c+\left[-\left(\dot{v}_{t1}-\dot{\theta}_cl_c\right)+\left(\dot{v}_{t2}+\dot{\theta}_cl_c\right)\right]C_{s2}l_c \\ &+\left[-\left(v_{t1}-\theta_cl_c\right)+\left(v_{t2}+\theta_cl_c\right)\right]K_{s2}l_c=0 \end{aligned} \quad (2)$$

For the vertical and pitch motions of the front and rear bogies:

$$\begin{aligned} &M_t\ddot{v}_{tj}-\left(v_c-v_{tj}\right)K_2-\left(\dot{v}_c-\dot{v}_{tj}\right)C_2+ \\ &\left[\left(\dot{v}_{tj}-\dot{v}_{w(2j-1)}\right)+\left(\dot{v}_{tj}-\dot{v}_{w(2j)}\right)\right]C_1+ \qquad ,j=1,2 \\ &\left[\left(v_{tj}-v_{w(2j-1)}\right)+\left(v_{tj}-v_{w(2j-1)}\right)\right]K_1=-M_tg \end{aligned} \quad (3)$$

$$\begin{cases} J_t\ddot{\theta}_{tj}+\left[-\left(\dot{v}_{w(2j-1)}-\dot{\theta}_{tj}l_t\right)+\left(\dot{v}_{w(2j)}+\dot{\theta}_{tj}l_t\right)\right]C_1l_t+ \\ \left[-\left(v_{w(2j-1)}-\theta_{tj}l_t\right)+\left(v_{w(2j)}+\theta_{tj}l_t\right)\right]K_1l_t=0 \qquad ,j=1 \\ J_t\ddot{\theta}_{tj}+\left[-\left(\dot{v}_{w(2j-1)}+\dot{\theta}_{tj}l_t\right)+\left(\dot{v}_{w(2j)}-\dot{\theta}_{tj}l_t\right)\right]C_1l_t+ \\ \left[-\left(v_{w(2j-1)}+\theta_{tj}l_t\right)+\left(v_{w(2j)}-\theta_{tj}l_t\right)\right]K_1l_t=0 \qquad ,j=2 \end{cases} \quad (4)$$

For the vertical motion of the wheels:

$$\begin{cases} M_{wi}\ddot{v}_{wi}-\left(\dot{v}_{tj}-\dot{v}_{wi}-\dot{\theta}_{tj}l_t\right)C_1- \\ \left(v_{tj}-v_{wi}-\theta_{tj}l_t\right)K_1=-M_wg+F_{hi} \qquad ,(i,j)=(1,1),(3,2) \\ M_{wi}\ddot{v}_{wi}-\left(\dot{v}_{tj}-\dot{v}_{wi}+\dot{\theta}_{tj}l_t\right)C_1- \\ \left(v_{tj}-v_{wi}+\theta_{tj}l_t\right)K_1=-M_wg+F_{hi} \qquad ,(i,j)=(2,1),(4,2) \end{cases} \quad (5)$$

In Equations (1-5), v and c represent the vertical and rotational freedoms, respectively. The subscripts *c, t, w, i* and *j* denote the car-body, bogies, wheel-sets, number of wheels, and number of bogies. The stiffness and damping are denoted by K and C with subscripts *1* or *2* for the primary and secondary suspension systems. M and J represent the mass and the moment of inertia. Based on these equations, the vehicle equation of motion in matrix form can be expressed as:

$$[M_v]\{\ddot{v}\}+[C_v]\{\dot{v}\}+[K_v]\{v\}=\{F_v(t)\} \quad (6)$$

Where $[M]$, $[C]$, and $[K]$ are the mass, damping, and stiffness matrices. $\{v\}$, $\{\dot{v}\}$, $\{\ddot{v}\}$, and F are the displacement, velocity, acceleration, and force vectors, respectively, with subscripts *v* denoting the train.

2.2 The lower subsystem model

The lower subsystem model in this study consists of two parts, including the track and the bridge, which are coupled by the interaction between the sleeper-rail and the ballast/bridge surface, as shown in Figure 3.

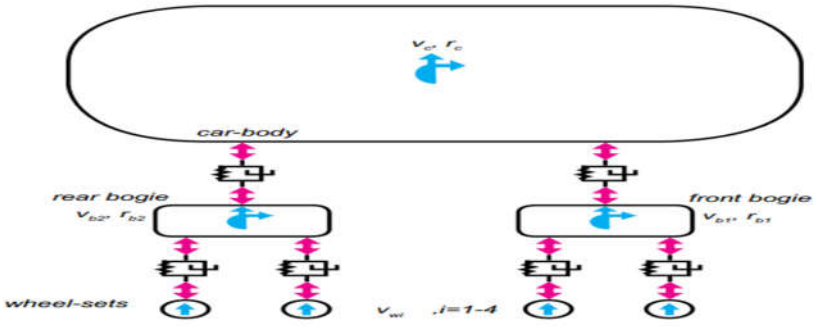

Figure 2. Model of the upper subsystem

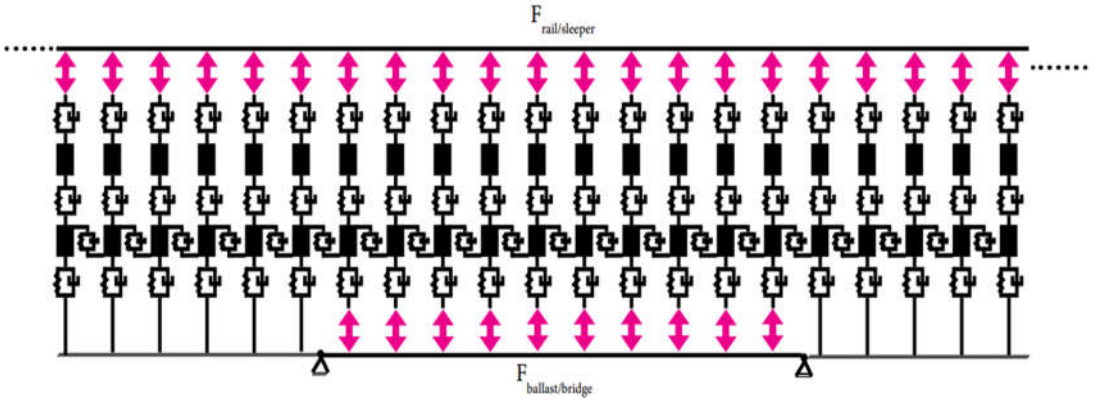

Figure 3. Model of lower subsystem

The lower subsystem is modeled using the finite element method. For this purpose, the track is modeled by the Euler-Bernoulli beam. The track structure, except for the rail, is modeled as rigid bodies, and the bridge is modeled by using the Timoshenko beam. The connecting elements are also modeled as linear spring-damper units. The separation between the ballast layer and the bridge is omitted. The lower subsystem coupled equation can be defined by:

$$\begin{bmatrix} M_r & 0 & 0 & 0 \\ & M_s & 0 & 0 \\ & & M_b & 0 \\ sym & & & M_{bi} \end{bmatrix} \begin{Bmatrix} \ddot{u}_r \\ \ddot{u}_s \\ \ddot{u}_b \\ \ddot{u}_{bi} \end{Bmatrix} + \begin{bmatrix} C_r & C_{r/s} & 0 & 0 \\ & C_s & C_{s/b} & 0 \\ & & C_b & C_{b/bi} \\ sym & & & C_{bi} \end{bmatrix} \begin{Bmatrix} \dot{u}_r \\ \dot{u}_s \\ \dot{u}_b \\ \dot{u}_{bi} \end{Bmatrix} + \begin{bmatrix} K_r & K_{r/s} & 0 & 0 \\ & K_s & K_{s/b} & 0 \\ & & K_b & K_{b/bi} \\ sym & & & K_b \end{bmatrix} \begin{Bmatrix} u_r \\ u_s \\ u_b \\ u_{bi} \end{Bmatrix} = \begin{Bmatrix} F_r + F_{w/r} \\ F_s \\ F_b \\ F_{bi} \end{Bmatrix} \quad (7)$$

Where subscripts *r, s, b,* and *bi* denote the rail, sleeper, ballast, and bridge elements, and the subscripts *r/s, s/b, b/bi* represent rail-sleeper, sleeper-ballast, and ballast/bridge interactions, respectively. Details of rail motion equations can be found in [16]. Also, the damping matrix, in Equation (7), is obtainable from Rayleigh damping by the linear combination of mass matrix and stiffness matrix of the bridge[17]:

$$[C_{bi}] = \alpha[M_{bi}] + \beta[K_{bi}] \quad (8)$$

Where:

$$\alpha = \frac{2\xi\omega_1\omega_2}{\omega_1 + \omega_2} \quad , \quad \beta = \frac{2\xi}{\omega_1 + \omega_2} \quad (9)$$

Where ω_1, ω_2 and ζ are the first and the second frequency and the damping ratio of the bridge, respectively.

2.3 Wheel/rail interaction

One of the critical elements of the dynamic analysis of the TTBI system is the link model between the wheel and the rail, which connects the two lower and upper subsystems [18]. Different models have been introduced by researchers to simulate and calculate the contact force between the wheel and the rail. Antolín et al [19] used the nonlinear model of the Hertzian spring to investigate the train-track interaction. Zakeri et al [20] also simplified the model by using the linear approach of wheel/rail contact in their study. In this study, the interaction between train and track model is considered as a nonlinear contact of wheel and rail surfaces. For this purpose, the wheel/rail interaction force is obtained by using a TTBI procedure. According to the nonlinear elastic Hertzian contact theory, the interaction force between *ith* wheel and rail at location *x* can be expressed as:

$$F^i_{w/r}(t) = \begin{cases} \left(\frac{1}{c_h} \left(|v_{wi} - (v_x + r_x)| \right) \right)^{3/2} & v_{wi} - (v_x + r_x) \le 0 \\ 0 & v_{wi} - (v_x + r_x) > 0 \end{cases} \quad (10)$$

Where v_{wi}, v_x and r_x are the displacements of *ith* wheel-set, rail displacement, and irregularity of rail surface in the coordinate *x*, respectively.c_h is the Hertzian contact coefficient determined by the material properties and the wheel and rail profile. To calculate the wheel/rail force, an iterative procedure needs to be performed at each time step [21].

2.4 The model of the unsupported sleeper

One of the most important disadvantages of the ballasted pavement is the distortion of the geometric properties of the track during operation. In this case, the quality of the ballast layer can be considered as the most influential factor. This layer always undergoes changes during line operation, including uneven and inelastic settlements, crushing, and moving of ballast particles. The progress of these changes depends on factors such as the nature of the dynamic moving loads on the track, seasonal melting and freezing cycles, and the quality of track maintenance. Therefore, considering a combination of these factors, creating a gap between the sleeper and the ballast layer in some places is inevitable. Consequently, the sleeper is suspended in the track. This track defect leads to produce a significant vibration in the track structure as the wheel passes through this section. As shown in Figure 4, the gap between the two elements of the sleeper and the ballast prevents them from connecting to each other.

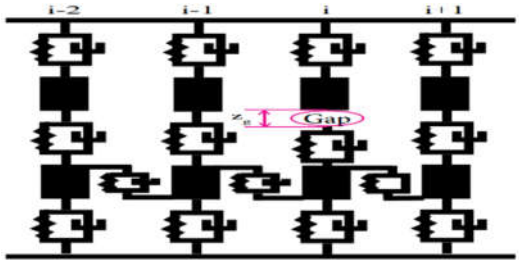

Figure 4. Illustration of the sleeper gap model

In this case, the contact force between the unsupported sleeper and ballast can be obtained by the following equation.

$$F^{i}_{s/b}=\begin{cases} k_b\left(\left|v_{si}-(v_{bi}+z_g)\right|\right)+ & v_{si}-(v_{bi}+z_g)\le 0 \\ c_b\left(\left|\dot{v}_{si}-\dot{v}_{bi}\right|\right) & \\ 0 & v_{si}-(v_{bi}+z_g)>0 \end{cases} \quad (11)$$

In Equation (11), $F^{i}_{s/b}$ is the contact force between the unsupported sleeper and ballast. k_b and c_b denote the stiffness and damping coefficient of the ballast layer, respectively. v_{si}, v_{bi} and z_g represent the vertical displacement of the unsupported sleeper and ballast and the gap size for *ith* interaction elements. $\dot{v}_{si}$ and $\dot{v}_{bi}$ are the vertical velocity of unsupported sleeper and the ballast bed for *ith* interaction elements.

2.5 Track irregularity

In TTBI calculation, track irregularities have a significant effect on the dynamic response of the system [22, 23]. In this study, to consider this factor, a random cluster of vertical irregularities recorded by the track recording car EM120 is used.The standard deviation index of the collected data is one. Figure 5 shows the sample taken for a length of 2000 meters.

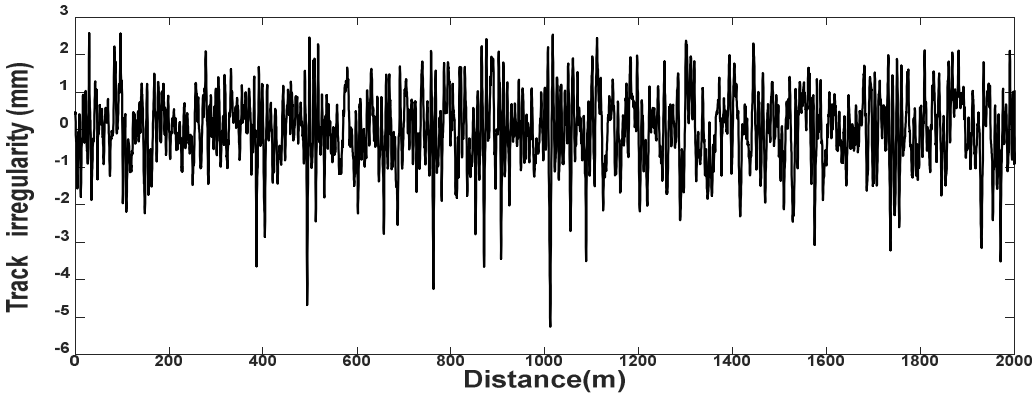

Figure 5. Track irregularity waves

2.6 Numerical solution method

In this study, the two subsystems' equations of motion need to be solved by numerical integration. The approach that is often used for the dynamic response of TTBI system is the Newmark-β method. Based on Newmark's finite difference scheme, displacement vector at time $t+dt$, ${}^{t+dt}u$, can be obtained by:

$$\begin{aligned}&(a_1[M]+a_3[C]+[K])\{{}^{t+dt}u\}=\\&\{{}^{t+dt}F\}+[M](a_1\{{}^{t}u\}+a_3\{{}^{t}\dot{u}\}+\\&a_4\{{}^{t}\ddot{u}\})+[C](a_3\{{}^{t}u\}+a_5\{{}^{t}\dot{u}\}+a_6\{{}^{t}\ddot{u}\})\end{aligned} \quad (12)$$

Respectively, velocity and acceleration at time step $t+dt$, can be evaluated by:

$$\{{}^{t+dt}\dot{u}\}=a_3(\{{}^{t+dt}u\}-\{{}^{t}u\})-a_5\{{}^{t}\dot{u}\}-a_6\{{}^{t}\ddot{u}\} \quad (13)$$

$$\{{}^{t+dt}\ddot{u}\}=a_1(\{{}^{t+dt}u\}-\{{}^{t}u\})-a_2\{{}^{t}\dot{u}\}-a_4\{{}^{t}\ddot{u}\} \quad (14)$$

Where the values of a_1 over a_6 can be defined as:

$$\begin{Bmatrix}a_1\\a_2\\a_3\\a_4\\a_5\\a_6\end{Bmatrix}=\begin{Bmatrix}1/(\alpha.dt^2)\\1/(\alpha.dt)\\\beta/dt\\1/(2\alpha)-1\\\beta/\alpha-1\\(1-\beta/(2\alpha)).dt\end{Bmatrix} \quad (15)$$

Where α and β are the parameters of Newmark's method. When $\alpha=0.25$ and $\beta=0.5$, the solution of the Newmark integration method is unconditionally stable [24], which means that convergence of the solver is assured, regardless of the size of the chosen time step.

2.7 Solution algorithm

To solve the dynamic equations of the upper and lower systems, the iterative cycle method can be used [25]. For this purpose, the procedures of the solution that is presented in Figure 6, and the following steps are taken:

1) The initial condition of the lower subsystem are defined as zero.
2) The interaction forces of the unsupported sleepers and ballast are considered to be zero, regardless of Equation (11).
3) The lower subsystem is analyzed under the moving loads of the train (Equation (7)).

Based on the response of the lower subsystem and taking into account the random irregularities, the upper subsystem is analyzed (Equation (6)).

4) Using the recorded history of the previous two steps, the wheel and rail interaction force is calculated (Equation (10)).
5) The performance of the unsupported sleeper is defined (Equation (11)).
6) The moving loads are replaced by the history of the wheels and rail nonlinear force. Then, the lower subsystem is analyzed under an updated condition.
7) The upper subsystem is analyzed by applying the lower subsystem response.

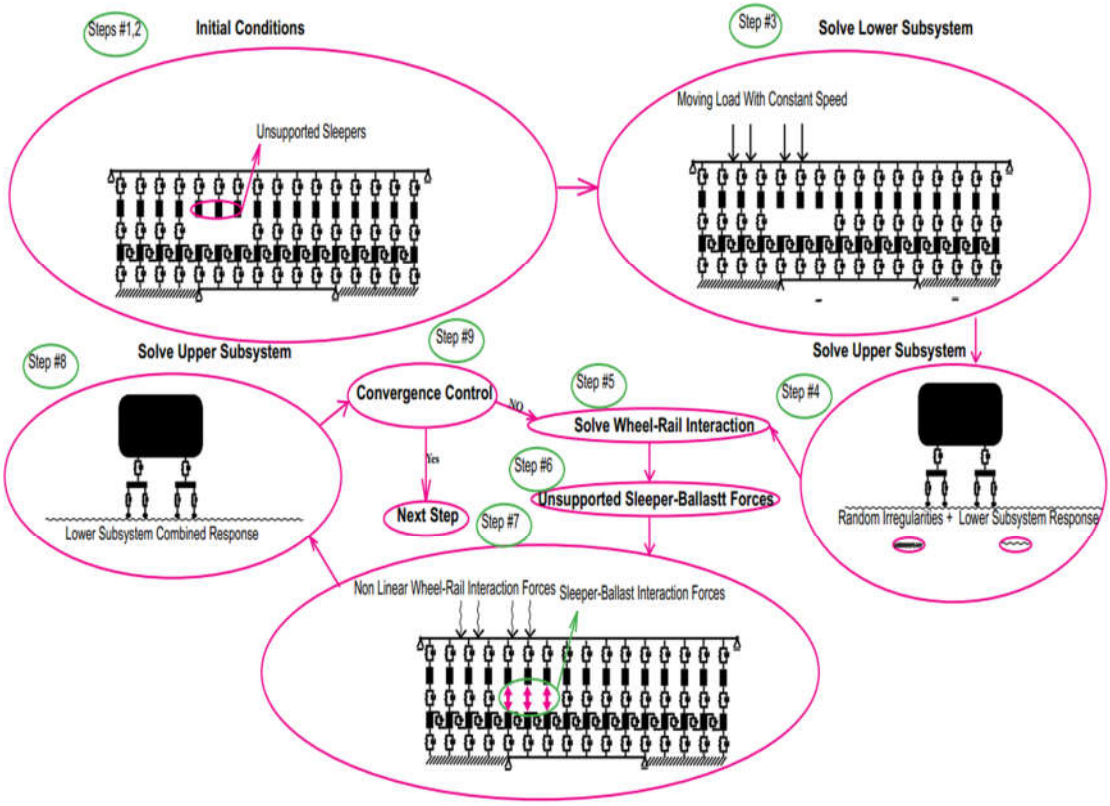

Figure 6. The procedure of dynamic analysis under unsupported sleepers

The convergence of the responses of both iterations is checked. For this purpose, according to Equation (16) from [26], if the relationship is verified, the next step of the analysis will be started. Otherwise, the process of calculations will be repeated from step 5.

$$\frac{Norm\left\{\Delta u\right\}_l^k}{Norm\left\{{}^t u_l^k\right\}} \le \varepsilon \tag{16}$$

Where:

$$\left\{\Delta u\right\}_l^k = {}^t u_l^k - {}^t u_l^{k-1} \tag{17}$$

$$norm\left\{\Delta u\right\}_l^k = \sum_{i=1}^{n}\left\{\Delta u^2{}_{(i)}\right\} \tag{18}$$

$$norm\left({}^t u_l^k\right) = \sum_{i=1}^{n}\left\{\left({}^t u_l^k\right)^2{}_{(i)}\right\} \tag{19}$$

Where ${}^t u_l^k$ and ${}^t u_l^{k-1}$ denote the lower displacement vector in time step (i) for both current and previous iteration, respectively. ε is a specified tolerance which in this research is set to 1×10^{-6}.

3.Verification

To verify the approach of TTBI solution, an example of a simply-supported bridge of length L = 30 m traveled by a moving vehicle from [27] is chosen. The properties of the bridge are listed in Table1. The model is shown in Figure 7. The vehicle properties are chosen from those for the Shinkansen train in [28], as listed in Table 2.The train speed is assumed to be 100 Km/h, which crosses the bridge at a constant speed. The track is modeled using a continuous Euler-Bernoulli beam on a series of horizontal and vertical spring-dampers. The results are compared to those from Ref [27, 29].

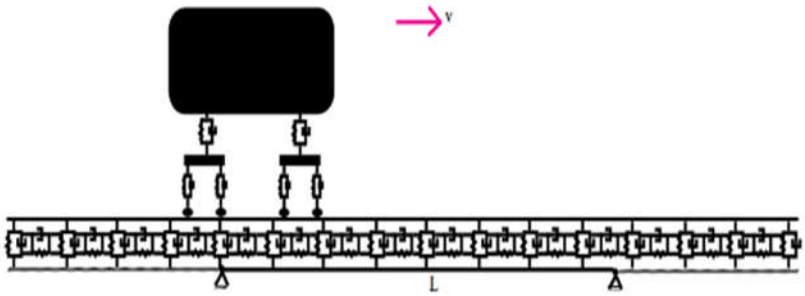

Figure 7. Moving sprung mass on the simply supported beam

Table 1. The bridge mechanical properties

Parameter	Notation	Value	Unit	Parameter	Notation	Value	Unit
Mass per meter	m_{bi}	41.74×10^{3}	Kg/m	Moment of inertia	I_{bi}	7.839	m^4
Young's modulus	E_{bi}	28.25×10^{9}	N/m^2	Section area	A_{bi}	8.730	Hz
				Poisson's ratio	v_{bi}	0.2	-

Table 2. Vehicle and Track properties

Vehicle

Parameter	Notation	Value	Unit	Parameter	Notation	Value	Unit
Mass of a car body	M_c	41.75×10^{3}	Kg	Primary suspension stiffness	K_1	1.18×10^{6}	N/m
Mass of a bogie	M_t	3.04×10^{3}	Kg	Secondary suspension stiffness	K_2	0.53×10^{6}	N/m
Mass of a wheel-set	M_w	1.78×10^{3}	Kg	Primary suspension damping	C_1	39.2×10^{3}	N.s/m
Pitch moment of inertia for bogie	J_c	2080×10^{3}	$Kg.m^2$	Secondary suspension damping	C_2	90.2×10^{3}	N.s/m
Pitch moment of inertia for car body	J_t	3.93×10^{3}	$Kg.m^2$	Distance from car body center to bogie center	l_c	8.75	m
				Distance from bogie center to wheel-set	l_t	1.25	m

Track

Parameter	Notation	Value	Unit	Parameter	Notation	Value	Unit
Mass per meter	m_t	587	Kg/m	Vertical stiffness	K_{vt}	240×10^{6}	N/m
Elastic modulus	E_t	2.1×10^{11}	N/m^2	Horizontal stiffness	K_{ht}	240×10^{6}	N/m
Moment of inertia	I_t	6.12×10^{-5}	m^4	Vertical damping	C_{vt}	58.8×10^{3}	N.s/m
				Horizontal damping	C_{ht}	58.8×10^{3}	N.s/m

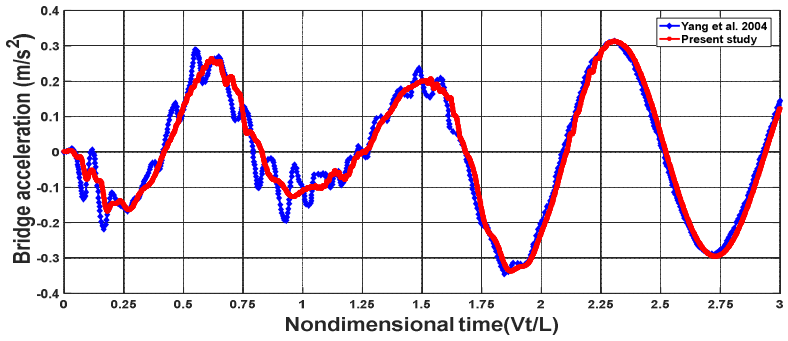

(a)

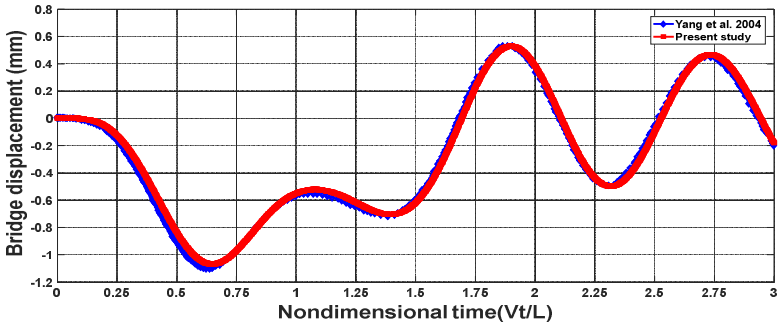

(b)

Figure 8. Dynamic response of bridge (a) midpoint acceleration (b) midpoint displacement

The dynamic response of the acceleration and displacement of the bridge are plotted in Figure 8. As the Figure suggests, there is a good agreement between the results of the numerical procedure used in this research and those published in [27].

4.Numerical Results and Discussions

The TTBI model that is proposed in this study is a powerful tool that can be used to investigate the dynamic response and vibrational performance of the railway bridge under a wide range of variations in the mechanical properties of railway components. The original purpose of this article is to study the effect of suspended sleepers on the dynamic performance of a concrete railway bridge. Since bridges are one of the most crucial parts of the rail network, strict regulations have been set for them in the railway standards. Therefore, this is considered a necessity for further study in this field. For this purpose, considering that the suspended sleepers can take place in any length of the bridge span, the dynamic model of the bridge is solved in the time domain. The advantage of this method is that it has a lower computational cost compared to the frequency domain. The upper subsystem concerned in this study is the ICE train composed of three vehicles with an average static axial load of approximately 100kN. The Track model is considered as three layers with a length of 32m, and the sleeper spacing is assumed to be 0.5m. The specific properties of the vehicle and track are adopted from Ref [30], as are listed in Table 3. In order to investigate the rail irregularities, a vertical recorded sample of the rail taken by the line measuring machine is considered in the calculation processes. The concrete bridge examined in this analysis is made of a 16-meter-long span. The mechanical characteristics of the bridge are similar to those published in Ref [31], as are summarized in Table 4. In this study, to increase the accuracy of the calculations, the time interval between two consecutive steps in the proposed algorithm is 10^{-3}s.

Table 3. Vehicle and Track properties

Vehicle							
Parameter	**Notation**	**Value**	**Unit**	**Parameter**	**Notation**	**Value**	**Unit**
Mass of a car body	M_c	49.5×10^3	Kg	Primary suspension stiffness	K_1	4.36×10^6	N/m
Mass of a bogie	M_t	10.7×10^3	Kg	Secondary suspension stiffness	K_2	1.72×10^6	N/m
Mass of a wheel-set	M_w	2.2×10^3	Kg	Primary suspension damping	C_1	220×10^3	N.s/m
Pitch moment of inertia for bogie	J_c	17.5×10^3	$Kg.m^2$	Secondary suspension damping	C_2	300×10^3	N.s/m
Pitch moment of inertia for car body	J_t	9.6×10^3	$Kg.m^2$	Distance from car body center to bogie center	l_c	8.75	m
				Distance from bogie center to wheel-set	l_t	1.25	m
Track							
Parameter	**Notation**	**Value**	**Unit**	**Parameter**	**Notation**	**Value**	**Unit**
Rail mass per meter	m_r	60	Kg/m	Foundation stiffness	K_f	130×10^6	N/m
Rail elastic modulus	E_r	12.1×10^{11}	N/m^2	Shear inter-locking stiffness	K_{sh}	20×10^6	N/m
Rail moment of inertia	I_r	3.22×10^{-5}	m^4	Fastener damping	C_p	248×10^3	N.s/m
Sleeper mass	m_s	320	Kg	Ballast damping	C_b	180×10^3	N.s/m
Ballast mass	m_b	1400	Kg	Foundation damping	C_f	62.3×10^3	N.s/m
Fastener stiffness	K_p	240×10^6	N/m	Shear inter-locking damping	C_{sh}	30×10^3	N.s/m
Ballast stiffness	K_b	70×10^6	N/m	Length of the rail element	l	0.5	m

Table 4. Bridge mechanical properties

Parameter	**Notation**	**Value**	**Unit**	**Parameter**	**Notation**	**Value**	**Unit**
Mass per meter	m_{bi}	31.4×10^3	Kg/m	Moment of inertia	I_{bi}	8.72	m^4
Young's modulus	E_{bi}	28.2×10^9	N/m^2	Section area	A_{bi}	7.94	m^2
Length of bridge	L_{bi}	16	m	Poisson's ratio	v_{bi}	0.2	-

In this research, the track – bridge interaction is discretized into a series of point-to-point interactions which are connected with linear spring and damping at each contact point.

4.1 Effect of unsupported sleepers group location along the bridge

One of the factors that need to be considered as the effect of unsupported sleepers on the dynamic response of the railway bridges is the

fact that this vibrational source may appear at any length of the bridge span. Therefore, a range of various positions of unsupported sleepers along the bridge span is analyzed. For this purpose, three consecutive sleepers are considered as a suspended sleeper-group. This group of unsupported sleepers is examined at certain distances of the bridge span. A 1 mm gap is provided between the suspended sleeper-group and the ballast layer. All calculations are performed under different suspended sleeper-group positions for train speeds of 140, 160, and 180 km / h. Figure 9 illustrates the maximum acceleration of the bridge versus the different positions of the suspended sleeper-group. From Figure 9, it can be found that at the two-eighth and five-eighth of the bridge span, the maximum of the bridge acceleration marks the peak value in all of the three cases of the train speed. Also, at the five-eighth of the bridge span, the maximum bridge acceleration has increased by approximately 100% compared to the case in which the suspended sleeper-group is located at the beginning of the bridge span. Comparing both bearings of the bridge, the peak of bridge acceleration for the suspended sleeper-group position at the end of the bridge is less than the beginning of the bridge. Figure 10 compares the time history of bridge acceleration in three cases; a fully supported sleeper-group, a suspended sleeper-group at the start of the bridge span, and also a suspended sleeper-group at the five-eighth location of the bridge span. The results were concluded from an analysis in which the speed of the train is 140 km/h, and also, a gap of 1 mm was considered for each case. From Figure 10, it can be concluded that the bridge acceleration amplitude for the case of suspended sleeper-group at the five-eighth location of the bridge span is by far higher than the two other cases. The maximum acceleration of the bridge for the cases of fully supported, the unsupported sleepers at the start and the five-eighth of the bridge span are equal to; 0.19, 0.29, and 0.58 m/s^2, respectively. Due to the increase in the bridge responses and limitations of the standards for the acceleration of the concrete bridges of the railway [32], the unsupported sleepers have a significant effect on the acceleration of the railway bridges, especially in a high-speed train.

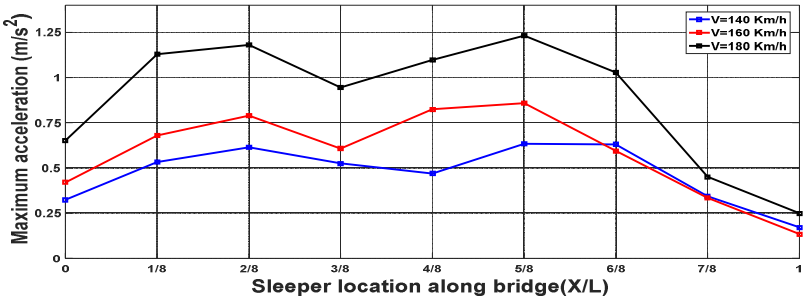

Figure 9. Maximum bridge acceleration response versus unsupported sleeper-group location

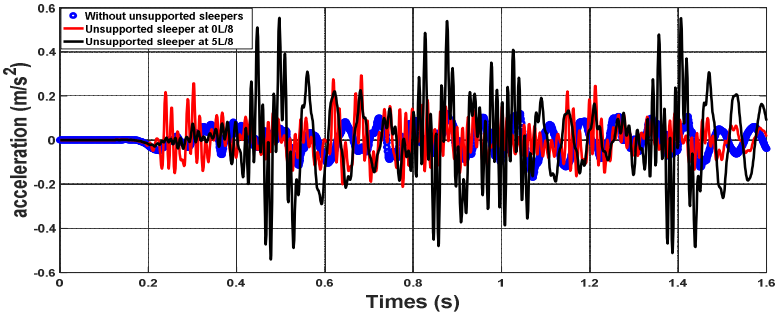

Figure 10. Time history of the bridge acceleration

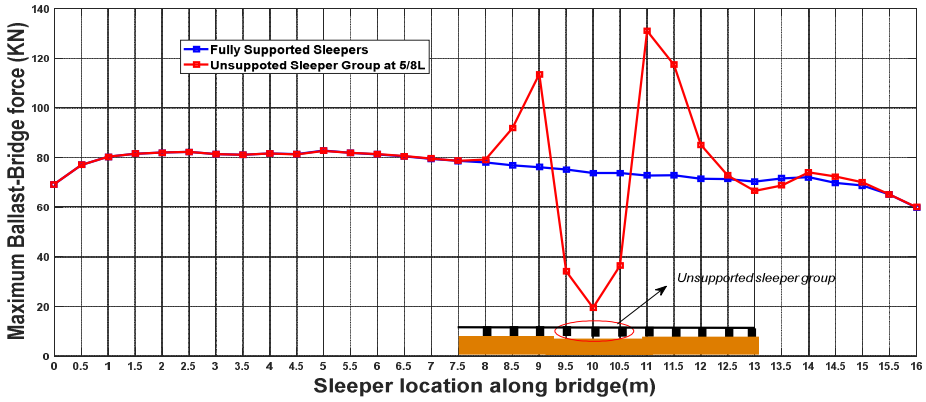

Figure 11. Maximum ballast–bridge interaction force versus the location of sleepers along the bridge

4.2 Effect of unsupported sleeper group on the force to the bridge

Figure 11 shows the interaction force between the sleepers and the ballast layer along the entire length of the bridge. The sleepers located at 9.5, 10, and 10.5m are unsupported. A 1 mm gap size for each unsupported sleeper is considered, and the rest of the sleepers are fully supported. As can be seen from Figure 11, the interaction forces for the first ballast/bridge element on both sides of the suspended sleeper-group have increased significantly, leading to growth between 45 and 60%, while for the suspended area, the ballast/bridge interaction is decreased. Also, looking at Figure 11 in more detail, it is known that the unsupported sleepers affect different lengths of the front and rear of the suspended area. The front area is covered by a large number of interaction points that are changed in the ballast/bridge interaction force. So the front area, in comparison with the rear area, affects the longer length of the bridge.

Comparing the contact forces in the front and rear, it can be found that the ballast/bridge interaction force has increased more in the front area than the rear area.

4.3 Effect of the train speed

To investigate the effect of different train speeds on the ballast acceleration, dynamic bridge response, and the wheel/rail interaction, a range of train speeds from 60 to 220 km/h is considered in this section. These studies are intended for three gap sizes of 0.8, 1.1, and 1.2 mm. The position of the suspended sleeper-group is considered at the five-eighth of the bridge span. Figure 12 illustrates the Influence of the train speed on the maximum acceleration of the sleepers for all three gap sizes. From Figure 12, it can be found that the maximum acceleration of sleeper increases as the train speed increases. By increasing the gap size by 0.2 mm, the maximum acceleration of sleeper increases by up to 20%.

The maximum acceleration of the bridge at different train speeds for the three different values of the gap is shown in Figure 13. It is clear that the maximum acceleration of the bridge increases by increasing the gap by 0.2mm, up to about 20% for the train speeds over 120Km/h. The wheel/rail interaction force is also studied as a vital element in the coupling of the lower and upper subsystems. Figure 14(a) shows the maximum wheel/rail interaction force for the three cases of gap sizes of 0.8, 1.0, and 1.2mm. The train speed is ranging from 60 to 220 km/h. The position of the suspended sleeper-group is considered at the five-eighth of the bridge span. From Figure 14(a), as the train speed increases, for speeds less than 180Km/h, the maximum of wheel/rail interaction force increases, and then reaches its peak at 180 km/h, and then decreases slightly. According to Figure 14(a), it can be concluded that by increasing the gap size by 0.2 mm, the contact force of the wheel/rail increases by up to 8-10%. Similar to the other two previous plots, the rate of change at higher speeds is faster. Also, Figure 14(b) illustrates the time history of the wheel/rail interaction forces around the suspended area.

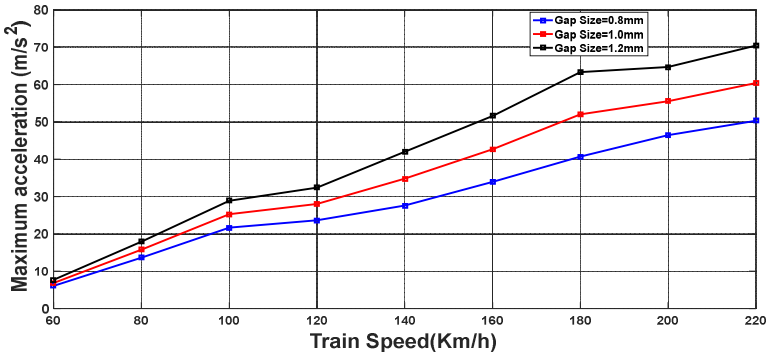

Figure 12. Maximum sleeper acceleration response versus train speed

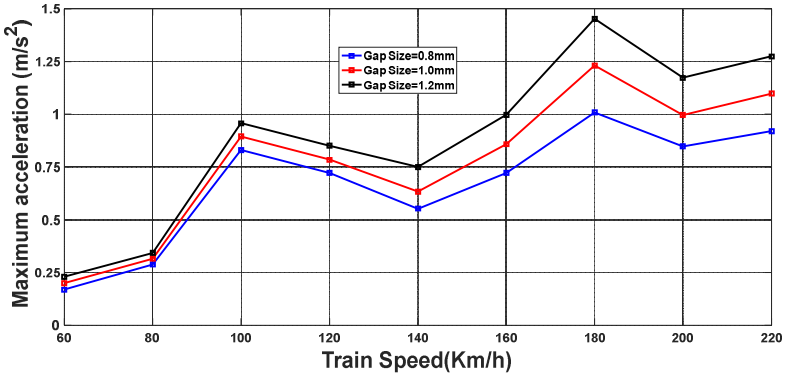

Figure 13. Maximum bridge acceleration response versus train speed

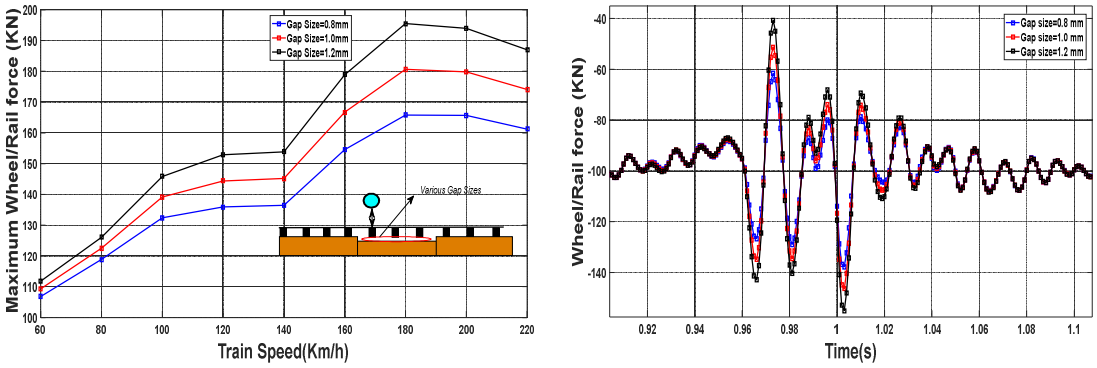

(a) (b)

Figure 14. Wheel/rail interaction force (a) the maximum wheel/rail interaction force versus train speed (b) time history of the wheel/rail interaction force

It can be found that the rate of increase for wheel/rail interaction is by far lower than the sleeper-ballast interaction rate, which concluded in section 4.1. Therefore, a group of unsupported sleepers can affect the lower subsystem more than the upper subsystem.

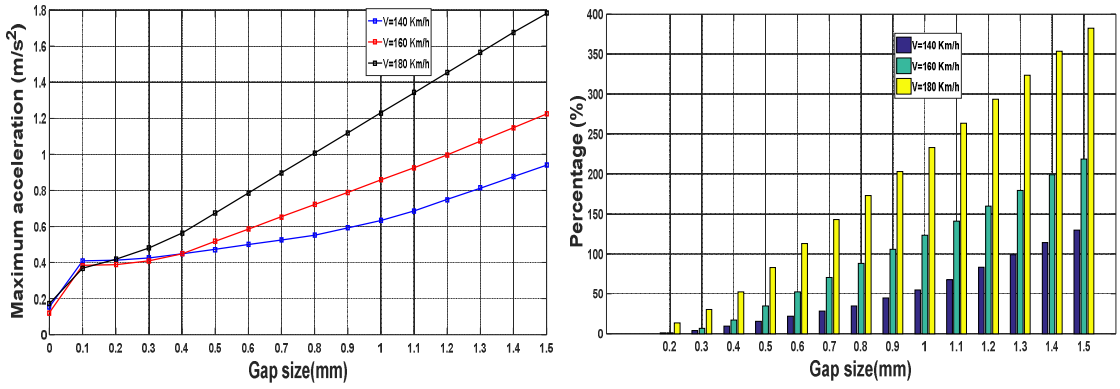

(a) (b)

Figure 15. Results of the bridge analysis (a) maximum of the bridge acceleration response (b) percentage of changes in the bridge response compared to a 0.1 mm gap size case

4.4 The effect of the gap size

In order to evaluate the effect of the gap size on the bridge dynamic responses, a study is performed on a group of 15 gap sizes from 0.1 mm to 1.5mm, as well as a fully supported sleeper-group case. All calculations are repeated for three train speeds of 140, 160, and 180 Km/h. The position of the suspended sleeper-group is considered at the five-eighth of the bridge span. According to Figure 15(a), the acceleration values of the 0.1 mm gap size are 0.38, 0.39, and 0.41 m/s^2, while in the 1.5mm case, these values are 0.93, 1.22, and 1.78 m/s^2, respectively. According to Figure 15(b), these increases are 138, 215, and 378 % of the maximum bridge acceleration for the 0.1 mm gap size, respectively. In addition, in Table 5, the bridge maximum acceleration changes are listed for gap sizes of 0.8, 1.1, and 1.2 mm. Looking at the last row of the table, adding 0.2 mm to the size of the gap, the maximum acceleration response of the bridge increases by up to 20%. The maximum interaction force between the ballast and the bridge is shown in Figure 16(a). From Figure 16(a), in the case of a 0.1 mm gap, the maximum of ballast/bridge interaction has increased by 35-40% compared to the fully supported case. The maximum interaction force of the ballast and the bridge versus the various gap size increases roughly linearly. As the train speed rises, the slope of the contact force diagram increases. Also, according to Figure 16(a) in more detail, it can be understood that by increasing the size of the gap by 0.2 mm, the maximum ballast/bridge interaction force can be increased by up to 5%. Also, Figure 16(b) shows that the maximum of contact force for the 1.5 mm gap size at train speeds of 140, 160, and 180 km/h has increased by 28, 26, and 22 %, respectively, compared to the 0.1 mm gap. Also, by considering the changes in the height of the bar graph at different train speeds and the gap sizes, the effect of the train speed on larger gapes is more significant.

Table 5. Difference of the bridge response versus the train speed and the gap size

Train speed	140			160			180		
Gap size (mm)	0.8	1.0	1.2	0.8	1.0	1.2	0.8	1.0	1.2
Maximum bridge acceleration(m/s^2)	0.55	063	0.75	0.72	0.86	0.99	1.01	1.22	1.45
Difference	14.5%		19%	19.4%		15.12%	20%		19%

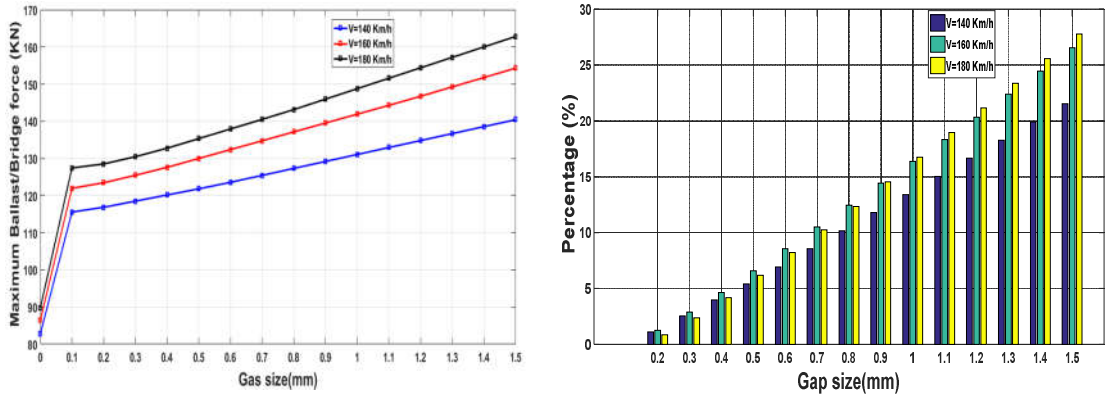

(a) (b)

Figure 16. Results of the ballast/bridge interaction force (a) maximum of the ballast/bridge interaction force (b) percentage of changes in the ballast/bridge interaction force compared to a 0.1 mm gap size case

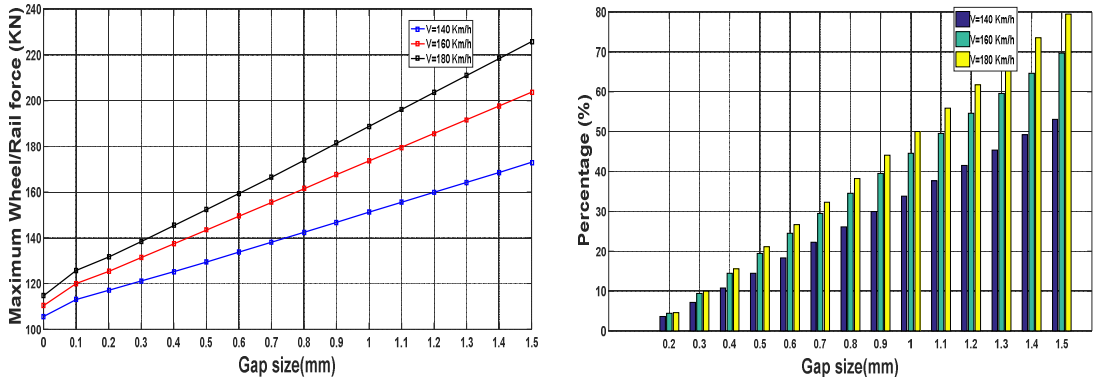

(a) (b)

Figure 17. Results of the wheel/rail interaction force (a) maximum of the wheel/rail interaction force (b) percentage of changes in the wheel/rail interaction force compared to a 0.1 mm gap size case

Figure 17(a) illustrates the rate of change in the contact force between the wheel and rail for different cases of the gap sizes. It is clear that as the train speed rises, the growth rate of the wheel and rail interaction increases. Also, from Figure 17(a), in the case of 0.2 mm gape size, the maximum of contact forces are 118, 125, and 131 KN, respectively, while for the 0.4 mm size, the values are increased to 124, 138, and 145 KN. It can be found that by increasing the gap size by 0.2 mm, the maximum wheel/rail interaction force can be increased by up to 10%, as the results of section 4.3. Also, Figure 17(b) shows the ratio of wheel and rail interaction changes for different gap sizes compared to the case of the 0.1 mm gap size. Examining the diagram, increasing the gap size by 0.1 mm, the wheel and rail contact force for the speed of 140, 160, and 180 Km/h are enhanced by 2, 3, and 5 %, respectively.

5.Conclusions

In this study, by considering a suspended sleeper group consisting of three consecutive unsupported sleepers, the dynamic response of a concrete bridge, the force applied to the bridge, as well as the contact force of the wheel and rail were investigated. The TTBI model in this study consisted of the two lower and upper subsystems. The two subsystems were coupled by nonlinear contact of the wheel and rail, and the final responses of the system were calculated under the multi-step algorithm presented in this

study. In order to analyze the problem, the suspended sleeper group was investigated at different positions along the length of the bridge span. Moreover, the effect of train speed and gap size on the response of TTBI, especially the bridge performance, was performed. The following results can be derived from the study.

1) For the case of the suspended sleeper-group located at 2/8 and 5/8 of the bridge span, the highest bridge responses occur. In this case, the maximum bridge acceleration can rise to twice of the suspended sleeper group located at the start of the bridge span.
2) In the area containing suspended traverses, the contact force between the rock and the bridge decreases, while on both sides of this area, the contact force increases. Also, in the front part of the suspended area, compared to the rear part: a) the longer length of the bridge is affected by the increase in contact force, b) The forces acting on the bridge increase to a higher percentage.
3) By increasing the size of the gap by 0.2 mm, the maximum acceleration of the bridge increases in the range of 10 to 20% for all three speeds of 140, 160, and 180 km/h. Moreover, the force applied to the bridge deck, sleeper acceleration, and the wheel /rail contact force increase by up to 5%, 20%, and 8-10%, respectively.

References

[1] Augustin, S., Gudehus, Gerd, Huber, Gerhard, Schünemann, Andreas, Numerical model and laboratory tests on settlement of ballast track, in System dynamics and long-term behaviour of railway vehicles, track and subgrade. 2003, Springer. p. 317-336.

[2] Li, Z. and J. Sun, Maintenance and cause of unsupported sleeper. China Railway Build, 1992. **2**: p. 15-17.

[3] Lammering, R. and M. Plenge, Investigations on railway tracks with special emphasis on partially unsupported sleepers due to voids. Engineering Transactions, 2000. **48**(3): p. 293–307.

[4] Zhu, Jian, Jun, Ahmed, A.K.W., Rakheja, Subhash, Khajepour, Amir, Development of a vehicle–track model assembly and numerical method for simulation of wheel–rail dynamic interaction due to unsupported sleepers. Vehicle system dynamics, 2010. **48**(12): p. 1535-1552.

[5] Zhang, Shuguang, Xiao, Xinbiao, Wen, Zefeng, Jin, Xuesong, Effect of unsupported sleepers on wheel/rail normal load. Soil Dynamics and Earthquake Engineering, 2008. **28**(8): p. 662-673.

[6] Zhu, J., D. Thompson, and C. Jones, On the effect of unsupported sleepers on the dynamic behaviour of a railway track. Vehicle system dynamics, 2011. **49**(9): p. 1389-1408.

[7] Lundqvist, A. and T. Dahlberg, Load impact on railway track due to unsupported sleepers. Proceedings of the Institution of Mechanical Engineers, Part F: Journal of Rail and Rapid Transit, 2005. **219**(2): p. 67-77.

[8] Bezin, Yann, Iwnicki, Simon, D., Cavalletti, M., De Vries, E., Shahzad, F., Evans, G, An investigation of sleeper voids using a flexible track model integrated with railway multi-body dynamics. Proceedings of the Institution of Mechanical Engineers, Part F: Journal of Rail and Rapid Transit, 2009. **223**(6): p. 597-607.

[9] Sadeghi, J., J.-A. Zakeri, and A.R. Tolou Kian. Effect of unsupported sleepers on rail track dynamic behaviour. in Proceedings of the Institution of Civil Engineers-Transport. 2018. Thomas Telford Ltd.

[10] Ishida, Makoto, Moto, Takuya, Kono, Akiko, Jin, Ying, Influence of loose sleeper on track dynamics and bending fatigue of rail welds. Quarterly report of RTRI, 1999. **40**(2): p. 80-85.

[11] Zakeri, J.A., M. Fattahi, and M.M. Ghanimoghadam, Influence of unsupported and partially supported sleepers on dynamic responses of train–track interaction. Journal of Mechanical Science and Technology, 2015. **29**(6): p. 2289-2295.

[12] Dai, Jian Ang, Kok Keng Jiang, Dongqi Luong, Van Hai Tran, Minh Thi, Dynamic response of high-speed train-track system due to unsupported sleepers. International Journal of Structural Stability and Dynamics, 2018. **18**(10): p. 1850122.

[13] Zakeri, Jabbar, Ali Fattahi, Morvarid Nouri, Mehrdad Janatabadi, Fatemeh, Influence of Rail Pad Stiffness and Axle Loads on Dynamic Responses of Train-track Interaction with Unsupported Sleepers. Periodica Polytechnica Civil Engineering, 2020. **64**(2): p. 524-534.

[14] Esmaeili, M., S.-A. Mosayebi, and J.-A. Zakeri, Ground-borne vibrations caused by

unsupported railway sleepers in ballasted tracks. Procedia engineering, 2017. **199**: p. 2645-2650.

[15] Stark, TD Wilk, ST Thompson, HB Sussmann, TR, Effect of unsupported ties at transition zones. Proceedings of Railway Engineering, 2015. **13**.

[16] Lei, X., High speed railway track dynamics: models, algorithms and applications. 2016: Springer.

[17] Pradelok, Stefan, Jasiński, Marcin, Kocański, Tomasz, Poprawa, Grzegorz, Numerical determination of dynamic response of the structure on the example of arch bridge. Procedia engineering, 2016. **161**: p. 1084-1089.

[18] Zhang, N., H. Xia, and W. Guo, Vehicle–bridge interaction analysis under high-speed trains. Journal of Sound and Vibration, 2008. **309**(3-5): p. 407-425.

[19] Antolín, Pablo, Zhang, Nan, Goicolea, José, M., Xia, He, Astiz, Miguel, Á., Oliva, Javier, Consideration of nonlinear wheel–rail contact forces for dynamic vehicle–bridge interaction in high-speed railways. Journal of Sound and Vibration, 2013. **332**(5): p. 1231-1251.

[20] Zakeri, J.A., H. Xia, and J.J. Fan, Dynamic responses of train-track system to single rail irregularity. Latin American Journal of Solids and Structures, 2009. **6**(2): p. 89-104.

[21] Andersson, Robin, Torstensson, Peter T., Kabo, Elena, Larsson, Fredrik, The influence of rail surface irregularities on contact forces and local stresses. Vehicle system dynamics, 2015. **53**(1): p. 68-87.

[22] Guo, WW., Xia, H., De Roeck, Guido, Liu, K., Integral model for train-track-bridge interaction on the Sesia viaduct: Dynamic simulation and critical assessment. Computers & Structures, 2012. **112**: p. 205-216.

[23] Klasztorny, M. and M. Podworna, Influence of random track irregularities on dynamic response of bridge/track structure/high-speed train systems. Journal of Civil Engineering and Architecture, 2014. **8**(10).

[24] Mohammadzadeh, S., S. Ahadi, and H. Keshavarzian, Assessment of fracture reliability analysis of crack growth in spring clip type Vossloh SKL14. Proceedings of the Institution of Mechanical Engineers, Part O: Journal of Risk and Reliability, 2014. **228**(5): p. 460-468.

[25] Yang, F. and G.A. FONDER, An iterative solution method for dynamic response of bridge–vehicles systems. Earthquake engineering & structural dynamics, 1996. **25**(2): p. 195-215.

[26] Cheng, Xiaohui, Jing, Weipeng, Song, Xianhua, Lu, Zeguang, Data Science: 5th International Conference of Pioneering Computer Scientists, Engineers and Educators, ICPCSEE 2019, Guilin, China, September 20–23, 2019, Proceedings. Vol. 1058. 2019: Springer Nature.

[27] Yang, Yeong-Bin, Yau, JD., Yao, Zhongda, Wu, YS., Vehicle-bridge interaction dynamics: with applications to high-speed railways. 2004: World Scientific.

[28] Wakui, Hajime, Matsumoto, Nobuyuki, Matsuura, Akio, Tanabe, Makoto, Dynamic interaction analysis for railway vehicles and structures. Doboku Gakkai Ronbunshu, 1995. **1995**(513): p. 129-138.

[29] Biggs, J.M. and J.M. Biggs, Introduction to structural dynamics. 1964: McGraw-Hill College.

[30] Zakeri, J.A. and H. Xia, Sensitivity analysis of track parameters on train-track dynamic interaction. Journal of Mechanical science and Technology, 2008. **22**(7): p. 1299-1304.

[31] Kargarnovin, M.H., Younesian, D., Thompson, D., Jones, C., Ride comfort of high-speed trains travelling over railway bridges. Vehicle System Dynamics, 2005. **43**(3): p. 173-197.

[32] Code, U., 776-2. Design requirements for rail-bridges based on interaction phenomena between train, track and bridge. International Union of Railways, 2009.

[33] Abe, N., Fukui, Y., Nagafuji, T., Ishida, M., Miura, S., Maintenance of rail welded part by grinding its irregularities for elongation of rail service life. Rep. Railw. Tech. Res. Inst, 1994. **8**(11): p. 17-22.

[34] Hamidi, S.A.J.a.p.a., On Sensitivity of Time Step for Dynamic Analysis of Bridges under Moving Loads. 2015.

[35] TB10002. 1-, J., Fundamental code for design on railway bridge and culvert. 2005, China Railway Publishing House Beijing.